Eur. Phys. J. C (2025) 85:500
https://doi.org/10.1140/epjc/s10052-025-14237-3

THE EUROPEAN PHYSICAL JOURNAL C

Regular Article - Theoretical Physics

Exploring vector-like top quark pair production via charged Higgs decays in multi-b-jet and opposite-sign dilepton final state at the LHC

R. Benbrik[1,a], **M. Berrouj**[1,b], **M. Boukidi**[1,2,c], **K. Kahime**[3,d]

[1] Polydisciplinary Faculty, Laboratory of Physics, Energy, Environment, and Applications, Cadi Ayyad University, B.P. 4162, Safi, Morocco
[2] Institute of Nuclear Physics, Polish Academy of Sciences, ul. Radzikowskiego 152, 31-342 Kraków, Poland
[3] Laboratoire Interdisciplinaire de Recherche en Environnement, Management, Energie et Tourisme (LIREMET), ESTE, Cadi Ayyad University, B.P. 383, Essaouira, Morocco

Received: 8 February 2025 / Accepted: 25 April 2025

Abstract We investigate the discovery prospects of a vector-like top partner (VLT) in the Type-II Two-Higgs-Doublet Model (2HDM-II) extended by a vector-like quark (VLQ) doublet (TB) at the 14 TeV Large Hadron Collider (LHC). In this work, the VLT is pair-produced via $pp \to T\bar{T}$ and predominantly decays through the cascade $T \to H^+ b \to tbb$, with the top quark decaying leptonically. The resulting final state, comprising an opposite-sign lepton pair and multiple b-jets, offers a clean experimental signature. We evaluate the discovery significance as a function of the VLT and charged Higgs masses, integrated luminosity, and background systematic uncertainties. For $m_{H^\pm} = 600$ GeV and 5% systematic uncertainty, a 5σ discovery is achievable for $m_T \lesssim 1300$ GeV with 300 fb^{-1} luminosity. At higher luminosities of 1000 and 3000 fb^{-1}, the reach extends to 1500–1600 GeV, depending on the level of systematic uncertainty. While heavier $H^\pm$ masses reduce sensitivity, discovery remains attainable at high luminosity.

1 Introduction

The discovery of the Higgs boson by the ATLAS and CMS collaborations at the Large Hadron Collider (LHC) [1,2] confirmed the Higgs mechanism as the cornerstone of electroweak symmetry breaking in the Standard Model (SM). Despite its success, the SM leaves several fundamental questions unanswered, including the nature of the scalar sector, the hierarchy problem, and the absence of a viable dark matter candidate. These open issues strongly motivate the exploration of extended Higgs sectors, among which the Two-Higgs-Doublet Model (2HDM) [3,4] stands out as a minimal and well-defined framework. The 2HDM predicts additional scalar states: a heavy CP-even Higgs (H), a CP-odd scalar (A), and a charged pair $(H^\pm)$, whose observation would constitute a clear signal of physics beyond the SM.

A particularly compelling extension of the 2HDM involves the addition of vector-like quarks (VLQs) [5–19] heavy colored fermions whose left- and right-handed components transform identically under the SM gauge group. VLQs arise naturally in many ultraviolet-complete frameworks, including extra-dimensional theories [20,21], composite Higgs models [22,23], and Grand Unified Theories (GUTs) [24]. Their gauge-invariant masses and non-standard Yukawa couplings allow interactions with both SM and BSM Higgs fields, opening new decay channels unrelated to electroweak symmetry breaking.

Among the most distinctive collider signatures in this framework are VLQ decays into non-standard Higgs bosons predicted by the 2HDM, such as $T/B \to H^\pm b/t$, Ht/b, or At/b [25–37]. These channels remain largely unexplored in existing LHC searches, which primarily focus on SM-like final states involving W, Z, or h bosons. Although current ATLAS and CMS searches have set stringent limits on VLQ masses [38], these bounds assume dominant decays into SM particles. The absence of signals in these conventional channels may, therefore, indicate substantial branching ratios into BSM scalars. Moreover, the interplay between the extended scalar and fermion sectors can induce loop-level cancellations that relax electroweak precision constraints, thereby

[a] e-mail: r.benbrik@uca.ac.ma
[b] e-mail: mbark.berrouj@ced.uca.ma
[c] e-mail: mohammed.boukidi@ced.uca.ma (corresponding author)
[d] e-mail: Kahimek@gmail.com

enlarging the viable parameter space and enhancing theoretical consistency.

In this work, we investigate the discovery potential of a vector-like top quark (VLT) in the Type-II 2HDM extended by a VLQ doublet (TB). We focus on the pair production process $pp \to T\bar{T}$ at $\sqrt{s} = 14$ TeV, followed by the cascade decay $T \to H^+ b \to tbb$, with the top quark undergoing leptonic decay. This yields a distinctive final state with multiple b-jets and an opposite-sign lepton pair, offering a clean and promising signature to simultaneously probe both the VLT and the charged Higgs boson.

The remainder of this paper is organized as follows: Sect. 2 outlines the theoretical setup, simulation strategy, and applied constraints. Numerical results and discovery projections are presented in Sect. 3, followed by conclusions in Sect. 4.

2 Framework

This section provides a concise overview of the 2HDM-II + VLQ framework. We begin by revisiting the well-known $\mathscr{C}\mathscr{P}$-conserving scalar potential of the 2HDM, involving two Higgs doublets (Φ_1, Φ_2) subject to a softly broken discrete $\mathbb{Z}_2$ symmetry, $\Phi_1 \to -\Phi_1$, which is softly violated by dimension-2 terms [3,39]:

$$\begin{aligned}
\mathscr{V} = & m_{11}^2 \Phi_1^\dagger \Phi_1 + m_{22}^2 \Phi_2^\dagger \Phi_2 - \left(m_{12}^2 \Phi_1^\dagger \Phi_2 + \text{h.c.}\right) \\
& + \frac{1}{2}\lambda_1 \left(\Phi_1^\dagger \Phi_1\right)^2 + \frac{1}{2}\lambda_2 \left(\Phi_2^\dagger \Phi_2\right)^2 \\
& + \lambda_3 \Phi_1^\dagger \Phi_1 \Phi_2^\dagger \Phi_2 + \lambda_4 \Phi_1^\dagger \Phi_2 \Phi_2^\dagger \Phi_1 \\
& + \left[\frac{1}{2}\lambda_5 \left(\Phi_1^\dagger \Phi_2\right)^2 + \text{h.c.}\right]. \qquad (1)
\end{aligned}$$

All parameters in this potential are real. The two complex scalar doublets $\Phi_{1,2}$ can be rotated into a basis, $H_{1,2}$, where only one of them acquires a Vacuum Expectation Value (VEV). By employing the minimization conditions of the potential for EWSB, the 2HDM can be parametrized by seven independent quantities: m_h, m_H, m_A, $m_{H^\pm}$, $\tan\beta = v_2/v_1$, $\sin(\beta - \alpha)$, and the soft-breaking parameter m_{12}^2

To suppress tree-level Flavor Changing Neutral Currents (FCNCs), the 2HDM admits four distinct Yukawa configurations, depending on how the $\mathbb{Z}_2$ symmetry is extended to the fermion sector.[1] These configurations are: Type-I, where Φ_2 couples to all fermions, Type-II, where Φ_2 couples to up-type quarks and Φ_1 to down-type quarks and charged leptons, Type-Y (Flipped), where Φ_2 couples to up-type quarks and charged leptons, and Φ_1 to down-type quarks, and Type-X (Lepton Specific), where Φ_2 couples to quarks, and Φ_1 to charged leptons.

Next, we introduce the VLQ component of the model. The gauge-invariant interactions between the new VLQs and SM particles arise from renormalizable couplings, with the VLQ representations specified as follows:

$$\begin{aligned}
& T^0_{L,R} && \text{(singlets)}, \\
& (X\,T^0)_{L,R}, \quad (T^0\,B^0)_{L,R} && \text{(doublets)}, \\
& (X\,T^0\,B^0)_{L,R}, \quad (T^0\,B^0\,Y)_{L,R} && \text{(triplets)}. \qquad (2)
\end{aligned}$$

In this context, the superscript zero distinguishes weak eigenstates from mass eigenstates. The electric charges of the VLQs are $Q_T = 2/3$, $Q_B = -1/3$, $Q_X = 5/3$, and $Q_Y = -4/3$, with T and B sharing the same electric charges as the SM top and bottom quarks, respectively.

The physical up-type quark mass eigenstates may, in general, contain non-zero $Q^0_{L,R}$ components (where Q represents the VLQ field) when new fields $T^0_{L,R}$ and $B^0_{L,R}$ with non-standard isospin assignments are added to the SM. This scenario leads to deviations in their couplings to the Z boson. These deviations are constrained by atomic parity violation experiments and measurements of R_c at LEP [40], which impose stringent limits for the up and charm quarks but are comparatively less restrictive for the top quark.

In the $\mathbb{Z}_2$ basis, the Yukawa Lagrangian for the three SM quark generations $q_{Li} = (u^0_{Li}\ d^0_{Li})^T$ ($i = 1, 2, 3$) and a VLQ doublet $Q_{L,R} = (T^0\ B^0)^T_{L,R}$ is given by:

$$\begin{aligned}
\mathscr{L}_Y = & -y^u_{ij}\bar{q}_{Li}\tilde{\Phi}_2 u_{Rj} - y^d_{ij}\bar{q}_{Li}\Phi_1 d_{Rj} \\
& - y^u_{4j}\bar{Q}_L\tilde{\Phi}_2 u_{Rj} - y^d_{4j}\bar{Q}_L\Phi_1 d_{Rj} + \text{h.c.}, \qquad (3)
\end{aligned}$$

where $\Phi_1 = (H_d^+\ H_d^0)^T$ and $\Phi_2 = (H_u^+\ H_u^0)^T$ are the Higgs doublets, and $\tilde{\Phi}_2 = i\sigma_2\Phi_2^*$ is the conjugate Higgs doublet. The Yukawa couplings $y^{u,d}_{ij}$ describe the interactions between the SM quarks and the Higgs doublets, where $i, j = 1, 2, 3$. The couplings $y^{u,d}_{4j}$ represent the interactions between the VLQs and the SM quarks.

We assume that the VLQ doublet eigenstates dominantly mix with the third generation, as motivated by the natural mass hierarchy [41] and consistent with stringent experimental constraints from low-energy flavor-changing processes [42–45]. Therefore, the mixing with the first two generations can be neglected, and we set $y^{u,d}_{41} = y^{u,d}_{42} = 0$, retaining only $y^{u,d}_{43} \neq 0$.

The mixing between the third-generation SM quarks and the VLQs is governed by 2×2 unitary matrices $U^u_{L,R}$ and $U^d_{L,R}$, which relate the weak eigenstates to the mass eigenstates. For the up-type quarks t and T:

$$\begin{pmatrix} t_{L,R} \\ T_{L,R} \end{pmatrix} = \begin{pmatrix} \cos\theta^u_{L,R} & -\sin\theta^u_{L,R} e^{i\phi_u} \\ \sin\theta^u_{L,R} e^{-i\phi_u} & \cos\theta^u_{L,R} \end{pmatrix} \begin{pmatrix} t^0_{L,R} \\ T^0_{L,R} \end{pmatrix}, \qquad (4)$$

[1] This work specifically focuses on the Type-II 2HDM within the alignment limit [4], where the lightest neutral Higgs boson is identified with the discovered 125 GeV state.

and for the down-type quarks[2] b and B:

$$\begin{pmatrix} b_{L,R} \\ B_{L,R} \end{pmatrix} = \begin{pmatrix} \cos\theta^d_{L,R} & -\sin\theta^d_{L,R} e^{i\phi_d} \\ \sin\theta^d_{L,R} e^{-i\phi_d} & \cos\theta^d_{L,R} \end{pmatrix} \begin{pmatrix} b^0_{L,R} \\ B^0_{L,R} \end{pmatrix}. \quad (5)$$

The mass terms for these quarks in the weak eigenstate basis are:

$$\mathscr{L}_{\text{mass}} = -(\bar{t}^0_L \ \bar{T}^0_L) \begin{pmatrix} y^u_{33}\frac{v}{\sqrt{2}} & 0 \\ y^u_{43}\frac{v}{\sqrt{2}} & M^0 \end{pmatrix} \begin{pmatrix} t^0_R \\ T^0_R \end{pmatrix} - (\bar{b}^0_L \ \bar{B}^0_L) \begin{pmatrix} y^d_{33}\frac{v}{\sqrt{2}} & 0 \\ y^d_{43}\frac{v}{\sqrt{2}} & M^0 \end{pmatrix} \begin{pmatrix} b^0_R \\ B^0_R \end{pmatrix} + \text{h.c.}. \quad (6)$$

where $v = 246$ GeV is the Higgs vacuum expectation value (VEV), and M^0 is the bare VLQ mass term.[3]

In the TB doublet scenario, gauge invariance ensures that the off-diagonal elements $y^{u,d}_{34}$ vanish, leaving $y^{u,d}_{33}$ and $y^{u,d}_{43}$ as the only non-zero Yukawa couplings. The mass matrix is diagonalized by the mixing matrices U^q_L and U^q_R, which satisfy:

$$U^q_L \mathscr{M}^q (U^q_R)^\dagger = \mathscr{M}^q_{\text{diag}}, \quad (7)$$

where $\mathscr{M}^q$ represents the mass matrices in Eq. (6), and $\mathscr{M}^q_{\text{diag}}$ are their diagonalized forms.

The left- and right-handed mixing angles for the quarks are related by:

$$\tan\theta^u_L \approx \frac{m_t}{m_T}\tan\theta^u_R, \quad \tan\theta^d_L \approx \frac{m_b}{m_B}\tan\theta^d_R, \quad (8)$$

where m_t and m_b are the masses of the SM top and bottom quarks, and m_T and m_B are the VLQ masses.

The TB doublet scenario within the 2HDM-II framework provides a compelling avenue for exploring charged Higgs bosons through VLQ decays. In this setup, the VLT decays into a charged Higgs boson ($H^\pm$) and a bottom quark (b) with a substantial branching ratio [28]. The decay width[4] for the process $T \to H^+ b$ is given by:

$$\Gamma(T \to H^+ b) = \frac{g^2}{64\pi}\frac{m_T}{M_W^2}\lambda(m_T, m_b, M_{H^\pm})^{1/2} \times \left\{ (|Z^L_{Tb}|^2 \cot^2\beta + |Z^R_{Tb}|^2 \tan^2\beta) \times \left[1 + r_b^2 - r^2_{H^\pm}\right] + 4r_b \text{Re}(Z^L_{Tb}) Z^{R*}_{Tb} \right\}. \quad (9)$$

Here, $r_x = m_x/m_T$, where x refers to one of the decay products, and the function $\lambda(x, y, z)$ is defined as:

$$\lambda(x, y, z) \equiv (x^4 + y^4 + z^4 - 2x^2y^2 - 2x^2z^2 - 2y^2z^2), \quad (10)$$

and

$$Z^L_{Tb} = c^d_L s^u_L e^{-i\phi_u} + (s^{u2}_L - s^{u2}_R)\frac{s^d_L}{c^u_L}, \quad Z^R_{Tb} = \frac{m_b}{m_T}\left[c^d_L s^u_L + (s^{d2}_R - s^{d2}_L)\frac{c^u_L}{s^d_L}\right] \quad (11)$$

2.1 EWPOs in VLQ

EWPOs impose stringent constraints on the parameter space of new physics scenarios. In our 2HDM+VLQ framework, both the extended scalar and fermionic sectors contribute to the oblique parameters S and T, which encapsulate radiative corrections to electroweak gauge boson propagators. The scalar contributions from the 2HDM are well established in the literature and are adopted from Ref. [46]. The fermionic contributions from VLQs can be computed analytically following the method of Ref. [47], which is applicable to VLQ singlet and doublet representations, and has been employed in, e.g., Ref. [48].

In this work, we compute the complete one-loop contributions of VLQs to the S and T parameters using `FeynArts-3.11` [49,50] and `FormCalc-9.10` [51,52], employing dimensional regularization and the Passarino–Veltman decomposition for loop integrals. We have verified both analytically and numerically that the resulting expressions are ultraviolet finite and renormalization-scale independent. (Analytical expressions for the VLQ representation studied are provided in Ref. [29], see also Ref. [25].)

2.2 Theoretical and experimental bounds

In this section, we outline the constraints used to validate our results.

- **Unitarity** constraints require the S-wave component of the various (pseudo)scalar-(pseudo)scalar, (pseudo)scalar-gauge boson, and gauge-gauge bosons scatterings to be unitary at high energy [53].
- **Perturbativity** constraints impose the following condition on the quartic couplings of the scalar potential: $|\lambda_i| < 8\pi$ ($i = 1, \ldots 5$) [3].
- **Vacuum stability** constraints require the potential to be bounded from below and positive in any arbitrary direction in the field space, as a consequence, the λ_i parameters

[2] Measurements of R_b at LEP set constraints on the b mixing with the new fields that are stronger than for mixing with the lighter quarks d, s [45].

[3] This gauge-invariant mass term is independent of the Higgs mechanism. It can either appear directly in the Lagrangian or arise from a Yukawa coupling to a scalar singlet that acquires a large VEV $v' \gg v$.

[4] Detailed analytical expressions for the couplings are provided in the Appendix of Ref. [28].

should satisfy the conditions as [54,55]:

$$\lambda_1 > 0, \quad \lambda_2 > 0, \quad \lambda_3 > -\sqrt{\lambda_1\lambda_2}, \\ \lambda_3 + \lambda_4 - |\lambda_5| > -\sqrt{\lambda_1\lambda_2}. \tag{12}$$

- **Constraints from EWPOs**, implemented through the oblique parameters, S and T [56], require that, for a parameter point of our model to be allowed, the corresponding $\chi^2(S^{\text{2HDM-II}} + S^{\text{VLQ}},\ T^{\text{2HDM-II}} + T^{\text{VLQ}})$ is within 95% Confidence Level (CL) in matching the global fit results [57]:

$$S = 0.05 \pm 0.08, \quad T = 0.09 \pm 0.07, \\ \rho_{S,T} = 0.92 \pm 0.11. \quad (\text{For } U = 0) \tag{13}$$

  Note that unitarity, perturbativity, vacuum stability, as well as S and T constraints, are enforced through the public code `2HDMC-1.8.0`[5] [58].
- **Constraints from the SM-like Higgs-boson properties** are taken into account by using `HiggsSignal-3` [59, 60] via `HiggsTools-1.2` [61]. We require that the relevant quantities (signal strengths, etc.) satisfy $\Delta\chi^2 = \chi^2 - \chi^2_{\text{min}}$ for these measurements at 95% CL ($\Delta\chi^2 \leq 6.18$).
- **Constraints from direct searches at colliders**, i.e., LEP, Tevatron, and LHC, are taken at the 95% CL and are tested using `HiggsBouns-6` [62–65] via `HiggsTools`. Including the most recent searches for neutral and charged scalars. In addition, the loop contributions of VLQs to $h \to gg$ and $h \to \gamma\gamma$ have been analyzed in our previous study [25]. These effects are minimal due to the decoupling behavior of VLQs at higher masses and the constraints on the mixing angles ($s^u_{L,R} \sim 0.2$). Consequently, $\mathscr{BR}(h \to gg)$ and $\mathscr{BR}(h \to \gamma\gamma)$ decrease by up to 10% and 3%, respectively, primarily due to modifications in the $ht\bar{t}$ coupling, while the direct $hT\bar{T}$ contributions remain negligible. For a detailed discussion of these effects, we refer the reader to Ref. [25].
- **Constraints from** $b \to s\gamma$: As established in [28], the Type-II 2HDM typically requires the charged Higgs boson mass to exceed 580 GeV to satisfy $b \to s\gamma$ constraint. The introduction of VLQs into the 2HDM can relax this stringent requirement, particularly when larger mixing angles are considered. However, restrictions from EWPOs limit the extent of these mixing angles, permitting charged Higgs masses below 580 GeV. In typical scenarios, the charged Higgs mass remains around 580 GeV for the 2HDM+T singlet and approximately 360 GeV or higher for the 2HDM-II + TB doublet, though the potential for lower masses exists under these relaxed conditions.
- **LHC direct search constraints for VLQs**: The current LHC limits primarily target the SM decay modes of VLT, such as $T \to Wb$, ht, and Zt. In our scenario, however, additional decay channels like $T \to H^\pm b$, Ht, and At become relevant, which may influence these limits. To ensure accuracy, we incorporated the latest LHC limits [66,67] into our analysis. We implemented a stringent condition where only parameter points meeting the criterion $r = \sigma_{\text{theo}}/\sigma^{\text{LHC}}_{\text{obs}} < 1$ were retained, signifying that points with $r \geq 1$ are excluded at the 95% CL.

[5] The code has been adjusted to include new VLQ couplings, along with the integration of analytical expressions for S_{VLQ_s} and T_{VLQ_s} outlined in Ref. [25].

Table 1 Parameter ranges explored for the 2HDM + TB framework

Parameter	Range
m_h	125.09 GeV
m_A	[400, 800] GeV
m_H	[400, 800] GeV
$m_{H^\pm}$	[400, 800] GeV
t_β	[1, 20]
$s_{\beta-\alpha}$	1
m^2_{12}	$m^2_A s_\beta c_\beta$
m_T	[1000, 2000] GeV
s^u_L	[−0.8, 0.8]
s^d_R	[−0.8, 0.8]

3 Analysis and simulation

Our study focuses on the 2HDM+TB framework, which is particularly notable for its enhanced production of charged Higgs bosons through the dominant decay channel $T \to H^+b$. In the high-mass regime ($m_T > 1$ TeV), this decay mode reaches a branching ratio close to 100%, distinguishing it from other VLQ representations that typically exhibit multiple competing decay channels (see Ref. [25,28] for details).

We performed a systematic scan of the parameter space within the ranges specified in Table 1, ensuring compatibility with all relevant theoretical and experimental constraints. As shown in Fig. 1, the results clearly indicate that $T \to H^+b$ dominates the VLT decay pattern for $m_T > 1$ TeV.

To optimize the signal and achieve sizable values for both $\mathscr{BR}(T \to H^+b)$ and $\mathscr{BR}(H^+ \to tb)$ across the VLT mass spectrum, we selected four representative benchmark points with $m_T = 1209.30$, 1452.71, 1646.60, and 1877.38 GeV, as summarized in Table 2.

The primary signal process under consideration is $pp \to T\bar{T} \to 2\,H^\pm + 2b$, where each charged Higgs boson decays via $H^\pm \to tb$. The subsequent top-quark decays, $t \to Wb$ followed by $W \to \ell\nu$ ($\ell = e, \mu$), result in a final state char-

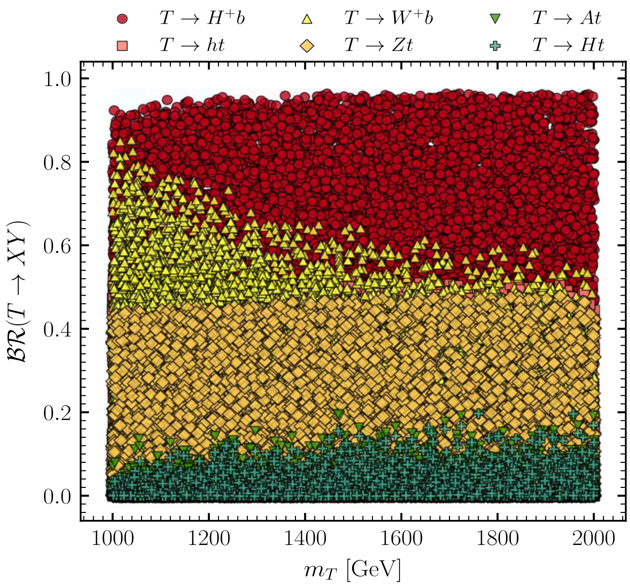

Fig. 1 $\mathscr{BR}(T \to XY)$ as a function of m_T, with $XY = H^+b$ (light blue), ht (salmon), Ht (blue), At (green), W^+b (yellow), and Zt (gold)

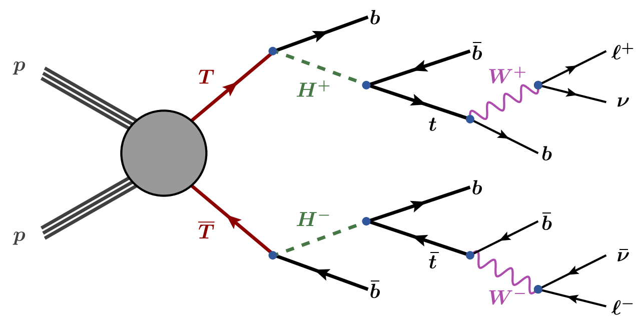

Fig. 2 Feynman diagrams for the pair production of VLT and their subsequent decays into an opposite-sign lepton pair final state, accompanied by multiple b-jets and missing transverse energy from neutrinos

acterized by multiple b-jets, an opposite-sign lepton pair, and missing transverse energy. Representative Feynman diagrams for the pair production and decay of VLTs are shown in Fig. 2. Given that the branching ratio $\mathscr{BR}(T \to H^+b)$ reaches values up to 98%, far exceeding the 34% maximum for $\mathscr{BR}(B \to H^+t)$ [26], the analysis focuses exclusively on $T\bar{T}$ production.

Event generation was performed using `MadGraph5_aMC@NLO` [68], while parton showering and hadronization were handled by `PYTHIA-8.2` [69]. Detector effects were simulated using `Delphes-3.4.2` [70], with jet reconstruction based on the anti-k_t algorithm [71] using a radius parameter $R = 0.4$ and a transverse momentum requirement of $p_T(b/j) > 20$ GeV. b-tagging efficiencies were applied following the `Delphes CMS` card [72].

For the parton distribution functions (PDFs), we employed the `NN23LO1` PDF set [73]. Background processes with high jet multiplicities were simulated using the MLM matching scheme [74] to ensure consistent merging of matrix element and parton shower calculations. To incorporate higher-order corrections, cross-sections were scaled by appropriate K-factors from the literature (Table 3). For the signal process, the next-to-next-to-leading-order (NNLO) K-factor was determined to be 1.42 using the `Top++` package [75].

After event generation, selection cuts were applied to enhance signal significance. Events were required to contain at least four b-jets satisfying:

– $p_T^{b/j} > 20$ GeV, $p_T^{\ell} > 10$ GeV,

Table 2 Benchmark points (BPs) for the 2HDM + TB framework. Masses are in GeV

Parameters	BP_1	BP_2	BP_3	BP_4
m_h	125.09	125.09	125.09	125.09
m_H	640.62	640.99	655.93	651.30
m_A	639.27	640.51	655.27	648.64
$m_{H\pm}$	642.49	648.62	647.40	671.88
t_β	5.51	5.04	4.22	5.22
$s_{\beta-\alpha}$	1	1	1	1
m_T	1209.30	1452.71	1646.60	1877.38
m_B	1217.69	1468.14	1662.59	1888.71
s_L^u	0.00008	0.00659	−0.00706	−0.00221
s_L^d	0.00046	−0.00051	−0.00045	−0.00028
s_R^u	0.00056	0.05536	−0.06717	−0.02405
s_R^d	0.11718	−0.15450	−0.15338	−0.11194
$\mathscr{BR}$ in %				
$\mathscr{BR}(T \to H^+b)$	93.98	93.49	91.43	95.19
$\mathscr{BR}(H^+ \to tb)$	95.63	96.86	98.33	96.42

Table 3 The K-factors of the QCD corrections for the background processes

Processes	$t\bar{t}b\bar{b}(j)$	$t\bar{t}jets$	$t\bar{t}W(j)$	$t\bar{t}Z(j)$	$t\bar{t}h(j)$	$t\bar{t}t\bar{t}$
K-factor	1.77 [76]	1.36 [77]	1.24 [78]	1.27 [79]	1.21 [80]	1.27 [81]

Table 4 Selection criteria for signal and background events at $\sqrt{s} = 14$ TeV

Cuts	Definition
Cut 1	$N(b) \geq 4, N(j) \geq 5, N(l^-) = 1, \ N(l^+) = 1$
Cut 2	$p_T(l^+) > 20, p_T(l^-) > 20$
Cut 3	$p_T(b_1) > 300, p_T(b_4) > 40$
Cut 4	$sp_T > 900$ GeV
Cut 5	$H_T > 1500$ GeV

– $|\eta^{b,j}| < 2.5$,
– $\Delta R(x, y) > 0.4$ for $x, y = j, b$.

The SM input parameters used are [82]:

$$m_t = 172.6 \text{ GeV}, \quad m_Z = 91.153 \text{ GeV},$$
$$\sin^2(\theta_W) = 0.2226, \quad \alpha(m_Z) = 1/127.934 \tag{14}$$

The analyzed observables include the number of b-tagged jets ($N[b]$) and light jets ($N[j]$), the total hadronic transverse energy $H_T = \sum_{\text{hadronic}} |\mathbf{p}_T|$, and the total transverse energy of reconstructed b-tagged jets (sp_T). The selection criteria applied to signal and background events are summarized in Table 4. Distributions for $N[b]$, $N[j]$, sp_T, and H_T for the signal benchmarks and backgrounds at $\sqrt{s} = 14$ TeV are presented in Fig. 3.

Table 5 presents the cut flows for signal and background events at $\sqrt{s} = 14$ TeV. The selection cuts effectively reduce the background while preserving high signal efficiency. After applying all cuts, the signal efficiencies are 9.58%, 13.01%, 14.71%, and 15.47% for BP_1, BP_2, BP_3, and BP_4, respectively, whereas background efficiencies are reduced to $\mathcal{O}(10^{-4})$ or lower.

The significance of the signal was evaluated using the median significance approach [83]. The discovery significance ($\mathcal{Z}_{\text{disc}}$) was calculated using the following formulas:

$$\mathcal{Z}_{\text{disc}} = \sqrt{2\left[(s+b)\ln\left(\frac{(s+b)\left(1+\delta^2 b\right)}{b+\delta^2 b\,(s+b)}\right) - \frac{1}{\delta^2}\ln\left(1+\delta^2\frac{s}{1+\delta^2 b}\right)\right]}, \tag{15}$$

where

$$x = \sqrt{(s+b)^2 - 4\delta^2 s b^2/\left(1+\delta^2 b\right)}.$$

To provide a comprehensive overview of the discovery prospects for VLTs, we extend our analysis to cover a mass range from 1000 GeV to 2000 GeV, building upon the characteristics of the previously discussed benchmark points. For each mass point, the discovery significance ($\mathcal{Z}_{\text{disc}}$) is evaluated at a center-of-mass energy of $\sqrt{s} = 14$ TeV, considering integrated luminosities of $\mathcal{L} = 300$ fb^{-1}, $\mathcal{L} = 1000$ fb^{-1}, and $\mathcal{L} = 3000$ fb^{-1}, alongside systematic uncertainties (δ) of 5%, 10%, and 20%. All evaluated points are consistent with theoretical and experimental constraints, ensuring the validity of the parameter space explored. Table 6 summarizes the discovery significances across the full mass range and luminosity scenarios.

For $\mathcal{L} = 300$ fb^{-1}, under $\delta = 5\%$ and 10%, the significance exceeds the discovery threshold ($\mathcal{Z}_{\text{disc}} \geq 5$) for m_T up to approximately 1300 GeV, with $\mathcal{Z}_{\text{disc}}$ values of 8.32 at 1000 GeV, 8.11 at 1100 GeV, 6.87 at 1200 GeV, and 5.49 at 1300 GeV. Under $\delta = 20\%$, discovery remains achievable up to $m_T = 1300$ GeV (with $\mathcal{Z}_{\text{disc}} = 5.28$), while for $m_T \geq 1400$ GeV the significance falls below the 5σ threshold.

At $\mathcal{L} = 1000$ fb^{-1} (HL-LHC), the discovery potential improves significantly. For $\delta = 5\%$ and 10%, $\mathcal{Z}_{\text{disc}}$ reaches values of 15.05 and 14.54, respectively, at $m_T = 1000$ GeV, and remains above 5 for masses up to about 1500 GeV. In the case of $\delta = 20\%$, the significance is slightly reduced, with discovery (i.e., $\mathcal{Z}_{\text{disc}} \geq 5$) being attainable up to approximately $m_T = 1400$ GeV.

At the maximal design goal of $\mathcal{L} = 3000$ fb^{-1}, the discovery reach is further extended. For $\delta = 5\%$ and 10%, $\mathcal{Z}_{\text{disc}}$ values remain well above 5 for masses up to about 1600 GeV (e.g., 25.47 at 1000 GeV, 21.12 at 1200 GeV, 16.96 at 1300 GeV, and 6.33 at 1600 GeV). Under $\delta = 20\%$, discovery is still viable up to $m_T \approx 1600$ GeV, with $\mathcal{Z}_{\text{disc}} = 5.33$ at 1600 GeV, while for $m_T \geq 1700$ GeV the significance drops below the discovery threshold.

Complementary to Table 6, Fig. 4 illustrates the significance as a function of m_T for three representative charged Higgs masses: $m_{H^\pm} = 600$, 800, and 1000 GeV. Horizontal grey lines denote the 5σ discovery and 95% confidence level (CL) exclusion thresholds. For $m_{H^\pm} = 600$ GeV, discovery-level significance ($\mathcal{Z}_{\text{disc}} \geq 5$) is attainable at an integrated luminosity of 300 fb^{-1} for T masses up to approximately 1300 GeV. As $m_{H^\pm}$ increases, the reach decreases due to the suppressed branching ratio BR($T \to H^+ b$), though discovery remains viable for $m_{H^\pm} = 800$ GeV over a slightly reduced m_T interval. For $m_{H^\pm} = 1000$ GeV, discovery is

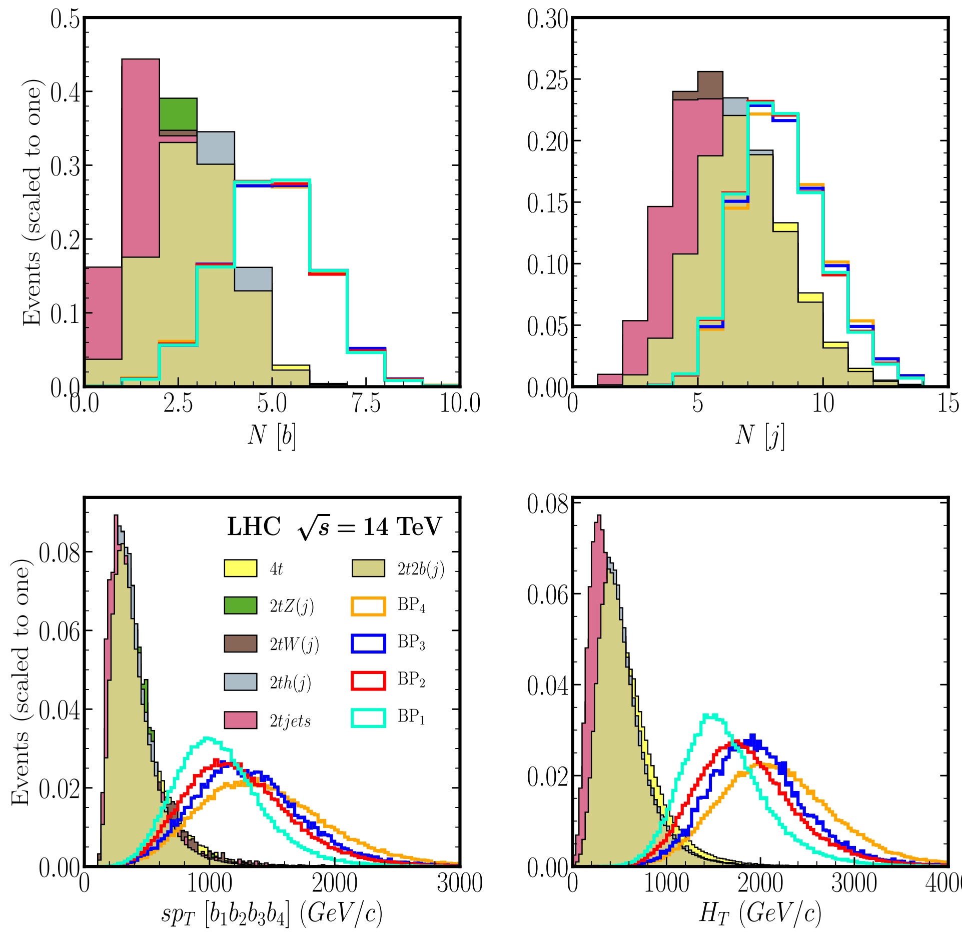

Fig. 3 Distributions of $N[b]$, $N[j]$, $sp_T(b_1b_2b_3b_4)$, and H_T for the signal benchmarks (BP_1, BP_2, BP_3, BP_4) and backgrounds at $\sqrt{s} = 14$ TeV

not feasible at 300 fb^{-1} but becomes accessible at higher luminosities, albeit over a narrower VLT mass range. These results underscore that charged Higgs masses below 1 TeV offer more favorable discovery prospects within the parameter space explored.

4 Discussion and summary

We have investigated the discovery prospects for a vector-like top partner (T) in the Type-II 2HDM extended by a VLQ doublet (TB) at the LHC. Our analysis focuses on the pair production process $pp \to T\bar{T}$ at $\sqrt{s} = 14$ TeV, followed by the cascade decay $T \to H^+b \to tbb$, with the top quark decaying leptonically. This results in a distinctive final state characterized by an opposite-sign lepton pair, multiple b-jets, and missing transverse energy.

Assuming a systematic uncertainty of 5%, we find that a 5σ discovery is achievable for T masses up to approximately 1300 GeV with an integrated luminosity of 300 fb^{-1}. For larger systematic uncertainties, up to 20%, the reach remains comparable. At 1000 fb^{-1}, the discovery potential extends to

Table 5 Cut flow for the signals and backgrounds at $\sqrt{s} = 14$ TeV, with cross sections in 10^{-2} fb

Cuts	Signals				Backgrounds					
	BP1	BP2	BP3	BP4	$2t2b(j)$	$2tjets$	$2tW(j)$	$2tZ(j)$	$2th(j)$	$4t$
Basic	33.81	7.30	5.98	0.84	5828.73	467702.09	43620.72	3462.61	2419.19	305.42
Cut1	7.34	1.59	1.26	0.18	31.33	105.60	0.10	3.13	11.06	3.16
Cut 2	6.29	1.36	1.11	0.16	26.46	81.92	0.08	2.48	9.90	2.53
Cut 3	5.34	1.25	1.02	0.15	2.37	5.45	0.01	0.21	0.65	0.42
Cut 4	4.57	1.12	0.96	0.14	0.531	1.81	0.0018	0.09	0.14	0.15
Cut 5	3.24	0.95	0.88	0.13	0.1416	0	0.0018	0	0	0.067
Efficiency	9.58%	13.01%	14.71%	15.47%	$2.42E^{-5}$	0	$4.12E^{-8}$	0	0	$1.73E^{-4}$

Table 6 Discovery significance, $\mathscr{Z}_{\rm disc}$, presented at varying systematic uncertainties (δ) and integrated luminosities ($\mathscr{L} = 300$ fb^{-1} $\mathscr{L} = 1000$ fb^{-1}, and $\mathscr{L} = 3000$ fb^{-1}). The parameters are fixed as follows: $m_H = 600.26$ GeV, $m_A = 595.24$ GeV, $m_{H^\pm} = 658.07$ GeV, $\tan\beta = 6$, $s_R^u = 0.05$, and $s_R^d = 0.11$. All points depicted are consistent with the discussed constraints

m_T [GeV]	$\mathcal{L} = 300$ fb^{-1}			$\mathcal{L} = 1000$ fb^{-1}			$\mathcal{L} = 3000$ fb^{-1}		
	$\delta = 5\%$	$\delta = 10\%$	$\delta = 20\%$	$\delta = 5\%$	$\delta = 10\%$	$\delta = 20\%$	$\delta = 5\%$	$\delta = 10\%$	$\delta = 20\%$
1000.0	8.32	8.22	7.90	15.05	14.54	13.11	25.47	23.41	19.08
1100.0	8.11	8.02	7.71	14.67	14.18	12.80	24.83	22.85	18.65
1200.0	6.87	6.80	6.57	12.44	12.08	10.99	21.12	19.58	16.13
1300.0	5.49	5.45	5.28	9.96	9.71	8.93	16.96	15.86	13.23
1400.0	4.07	4.05	3.95	7.40	7.24	6.74	12.63	11.94	10.13
1500.0	2.95	2.93	2.87	5.36	5.27	4.95	9.18	8.75	7.54
1600.0	2.03	2.02	1.99	3.69	3.64	3.45	6.33	6.08	5.33
1700.0	1.38	1.38	1.36	2.52	2.49	2.38	4.33	4.18	3.72
1800.0	0.93	0.93	0.92	1.69	1.68	1.61	2.91	2.82	2.54
1900.0	0.61	0.61	0.60	1.11	1.10	1.06	1.90	1.85	1.68
2000.0	0.40	0.40	0.40	0.73	0.73	0.70	1.26	1.23	1.12

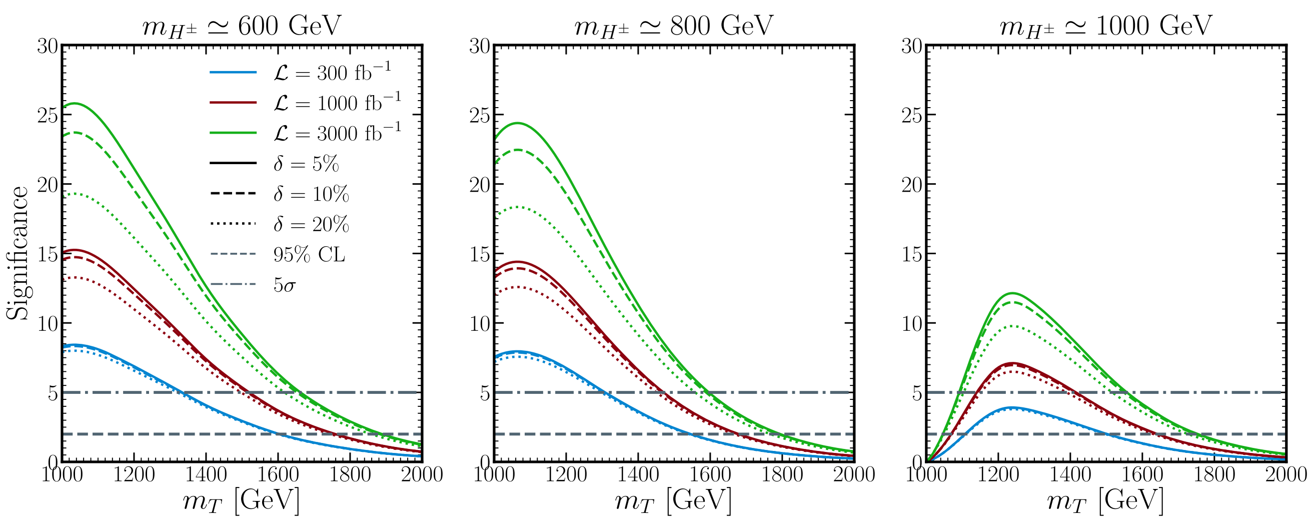

Fig. 4 Significance as a function of m_T for three benchmark charged Higgs masses: $m_{H^\pm} = 600$ GeV (left), 800 GeV (middle), and 1000 GeV (right), shown for different systematic uncertainties (δ) and integrated luminosities $\mathscr{L} = 300$, 1000, and 3000 fb^{-1}. The parameters are fixed to $m_H \simeq m_A \simeq m_{H^\pm}$, $\tan\beta = 5$, $s_R^u = 0.05$, and $s_R^d = 0.11$. All points depicted are consistent with the discussed constraints

1500 GeV for 5–10% systematics and to 1400 GeV for 20%. With the full HL-LHC luminosity of 3000 fb^{-1}, T masses up to 1600 GeV become accessible in all scenarios.

We have also examined the sensitivity as a function of the charged Higgs mass. For $m_{H^\pm} = 600$ GeV, discovery is already possible at 300 fb^{-1}. As $m_{H^\pm}$ increases, the branching ratio for $T \to H^+ b$ decreases, reducing the signal rate. For $m_{H^\pm} = 1000$ GeV, discovery is not viable at 300 fb^{-1} but becomes feasible at higher luminosities, though over a narrower T mass window. Specifically, masses between 1200–1400 GeV can be probed at 1000 fb^{-1}, and 1100–1600 GeV at 3000 fb^{-1}.

These results underscore the interplay between the scalar mass spectrum, integrated luminosity, and systematic uncertainties in shaping the discovery potential of extended Higgs sectors. The $T\bar{T}$ production mode, characterized by multiple b-jets and an opposite-sign lepton pair, offers a promising avenue for probing both VLQs and charged Higgs bosons in upcoming and future LHC runs.

Funding R. Benbrik is supported in part by the PIFI Grant No. 110200EZ52. M. Boukidi acknowledges the support of Narodowe Centrum Nauki under OPUS grant no. 2023/49/B/ST2/03862.

Data Availability Statement Data will be made available on reasonable request. [Authors' comment: The data used to generate the plots can be provided upon re- quest by contacting the authors of the manuscript.]

Code Availability Statement Code/software will be made available on reasonable request. [Authors' comment: Code/software sharing is not applicable to this article.]

References

1. ATLAS Collaboration, Observation of a new particle in the search for the Standard Model Higgs boson with the ATLAS detector at the LHC. Phys. Lett. B **716**, 1 (2012). https://doi.org/10.1016/j.physletb.2012.08.020. arXiv:1207.7214
2. CMS Collaboration, Observation of a new boson at a mass of 125 GeV with the CMS experiment at the LHC. Phys. Lett. B **716**, 30 (2012). https://doi.org/10.1016/j.physletb.2012.08.021. arXiv:1207.7235
3. G.C. Branco, P.M. Ferreira, L. Lavoura, M.N. Rebelo, M. Sher, J.P. Silva, Theory and phenomenology of two-Higgs-doublet models. Phys. Rep. **516**, 1 (2012). https://doi.org/10.1016/j.physrep.2012.02.002. arXiv:1106.0034
4. P. Draper, A. Ekstedt, H.E. Haber, A natural mechanism for approximate Higgs alignment in the 2HDM. JHEP **05**, 235 (2021). https://doi.org/10.1007/JHEP05(2021)235. arXiv:2011.13159
5. J.A. Aguilar-Saavedra, R. Benbrik, S. Heinemeyer, M. Pérez-Victoria, Handbook of vectorlike quarks: mixing and single production. Phys. Rev. D **88**, 094010 (2013). https://doi.org/10.1103/PhysRevD.88.094010. arXiv:1306.0572
6. M. Buchkremer, G. Cacciapaglia, A. Deandrea, L. Panizzi, Model independent framework for searches of top partners. Nucl. Phys. B **876**, 376 (2013). https://doi.org/10.1016/j.nuclphysb.2013.08.010. arXiv:1305.4172
7. B. Fuks, H.-S. Shao, QCD next-to-leading-order predictions matched to parton showers for vector-like quark models. Eur. Phys. J. C **77**, 135 (2017). https://doi.org/10.1140/epjc/s10052-017-4686-z. arXiv:1610.04622
8. J.A.M. Alves, G.C. Branco, A.L. Cherchiglia, C.C. Nishi, J.T. Penedo, P.M.F. Pereira et al., Vector-like singlet quarks: a roadmap. Phys. Rep. **1057**, 1 (2024). https://doi.org/10.1016/j.physrep.2023.12.004. arXiv:2304.10561
9. S. Gopalakrishna, T. Mandal, S. Mitra, G. Moreau, LHC signatures of warped-space vectorlike quarks. JHEP **08**, 079 (2014). https://doi.org/10.1007/JHEP08(2014)079. arXiv:1306.2656
10. L. Han, S. Wang, L. Shang, B. Yang, Search for the singlet vector-like top quark in the channel with at hadron colliders*. Chin. Phys. C **47**, 043108 (2023). https://doi.org/10.1088/1674-1137/acb994. arXiv:2302.14642
11. J.-Z. Han, Y.-B. Liu, S. Moretti, Searching for single production of vector-like quarks decaying into Wb at a future muon-proton collider. arXiv:2501.01026
12. J.-Z. Han, Y.-B. Liu, L. Xing, S. Xu, Search for single production of vectorlike B-quarks at the LHC*. Chin. Phys. C **46**, 103103 (2022). https://doi.org/10.1088/1674-1137/ac79ab. arXiv:2208.06845
13. B. Yang, X. Sima, S. Wang, L. Shang, Single vectorlike top quark production in the tZ channel at high energy pp colliders. Phys. Rev. D **105**, 096010 (2022). https://doi.org/10.1103/PhysRevD.105.096010
14. X.-Y. Tian, L.-F. Du, Y.-B. Liu, Single production of vector-like top partners in trilepton channel at future 100 TeV Hadron colliders. Nucl. Phys. B **965**, 115358 (2021). https://doi.org/10.1016/j.nuclphysb.2021.115358
15. B. Yang, J. Li, M. Wang, L. Shang, Search for the singlet vector-like lepton in semileptonic channel at future e^+e^- colliders. Phys. Rev. D **104**, 055019 (2021). https://doi.org/10.1103/PhysRevD.104.055019
16. J. Cao, L. Meng, L. Shang, S. Wang, B. Yang, Interpreting the W-mass anomaly in vectorlike quark models. Phys. Rev. D **106**, 055042 (2022). https://doi.org/10.1103/PhysRevD.106.055042. arXiv:2204.09477
17. B. Yang, Z. Li, X. Jia, S. Moretti, L. Shang, Search for single vector-like B quark production in hadronic final states at the LHC. arXiv:2405.13452
18. A. Banerjee, E. Bergeaas Kuutmann, V. Ellajosyula, R. Enberg, G. Ferretti, L. Panizzi, Vector-like quarks: status and new directions at the LHC. arXiv:2406.09193
19. A. Banerjee, V. Ellajosyula, L. Panizzi, Heavy vector-like quarks decaying to exotic scalars: a case study with triplets. JHEP **01**, 187 (2024). https://doi.org/10.1007/JHEP01(2024)187. arXiv:2311.17877
20. L. Randall, R. Sundrum, A large mass hierarchy from a small extra dimension. Phys. Rev. Lett. **83**, 3370 (1999). https://doi.org/10.1103/PhysRevLett.83.3370. arXiv:hep-ph/9905221
21. M. Carena, A.D. Medina, B. Panes, N.R. Shah, C.E.M. Wagner, Collider phenomenology of gauge-Higgs unification scenarios in warped extra dimensions. Phys. Rev. D **77**, 076003 (2008). https://doi.org/10.1103/PhysRevD.77.076003. arXiv:0712.0095
22. K. Agashe, R. Contino, A. Pomarol, The minimal composite Higgs model. Nucl. Phys. B **719**, 165 (2005). https://doi.org/10.1016/j.nuclphysb.2005.04.035. arXiv:hep-ph/0412089
23. R. Barbieri, B. Bellazzini, V.S. Rychkov, A. Varagnolo, The Higgs boson from an extended symmetry. Phys. Rev. D **76**, 115008 (2007). https://doi.org/10.1103/PhysRevD.76.115008. arXiv:0706.0432
24. J.L. Hewett, T.G. Rizzo, Low-energy phenomenology of superstring inspired E(6) models. Phys. Rep. **183**, 193 (1989). https://doi.org/10.1016/0370-1573(89)90071-9
25. A. Arhrib, R. Benbrik, M. Boukidi, B. Manaut, S. Moretti, Anatomy of vector-like top-quark models in the alignment limit of the 2-Higgs Doublet Model Type-II. Eur. Phys. J. C **85**, 2 (2025). https://doi.org/10.1140/epjc/s10052-024-13692-8. arXiv:2401.16219
26. A. Arhrib, R. Benbrik, M. Boukidi, S. Moretti, Anatomy of vector-like bottom-quark models in the alignment limit of the 2-Higgs doublet model type-II. Eur. Phys. J. C **84**, 1008 (2024). https://doi.org/10.1140/epjc/s10052-024-13390-5. arXiv:2403.13021

27. A. Arhrib, R. Benbrik, M. Boukidi, S. Moretti, Large hadron collider signatures of exotic vector-like quarks within the 2-Higgs doublet model type-II. arXiv:2409.20104
28. R. Benbrik, M. Boukidi, S. Moretti, Probing charged Higgs bosons in the two-Higgs-doublet model type II with vectorlike quarks. Phys. Rev. D **109**, 055016 (2024). https://doi.org/10.1103/PhysRevD.109.055016. arXiv:2211.07259
29. H. Abouabid, A. Arhrib, R. Benbrik, M. Boukidi, J.E. Falaki, The oblique parameters in the 2HDM with vector-like quarks: confronting M $_W$ CDF-II anomaly. J. Phys. G **51**, 075001 (2024). https://doi.org/10.1088/1361-6471/ad3f34. arXiv:2302.07149
30. R. Benbrik, M. Berrouj, M. Boukidi, Investigation of charged Higgs bosons production from vectorlike T quark decays at eγ collider. Phys. Rev. D **111**, 015027 (2025). https://doi.org/10.1103/PhysRevD.111.015027. arXiv:2408.15985
31. A. Arhrib, R. Benbrik, M. Berrouj, M. Boukidi, B. Manaut, Search for charged Higgs bosons through vector-like top quark pair production at the LHC. arXiv:2407.01348
32. R. Benbrik, M. Berrouj, M. Boukidi, A. Habjia, E. Ghourmin, L. Rahili, Search for single production of vector-like top partner $T \to H^+ b$ and $H^\pm \to tb$ at the LHC Run-III. Phys. Lett. B **843**, 138024 (2023). https://doi.org/10.1016/j.physletb.2023.138024
33. R. Benbrik, M. Boukidi, S. Moretti, Charged Higgs boson mass bounds in 2HDM-II: impact of vector-like quarks. PoS **ICHEP2024**, 083 (2025). https://doi.org/10.22323/1.476.0083. arXiv:2409.16054
34. J.A. Aguilar-Saavedra, D.E. López-Fogliani, C. Muñoz, Novel signatures for vector-like quarks. JHEP **06**, 095 (2017). https://doi.org/10.1007/JHEP06(2017)095. arXiv:1705.02526
35. R. Dermíšek, E. Lunghi, S. Shin, Hunting for vectorlike quarks. JHEP **04**, 019 (2019). https://doi.org/10.1007/JHEP04(2019)019. arXiv:1901.03709
36. A. Ghosh, P. Konar, Precision prediction at the LHC of a democratic up-family philic KSVZ axion model. arXiv:2305.08662
37. R. Benbrik et al., Signatures of vector-like top partners decaying into new neutral scalar or pseudoscalar bosons. JHEP **05**, 028 (2020). https://doi.org/10.1007/JHEP05(2020)028. arXiv:1907.05929
38. R. Benbrik, M. Boukidi, M. Ech-chaouy, S. Moretti, K. Salime, Q.-S. Yan, Vector-like quarks at the LHC: a unified perspective from ATLAS and CMS exclusion limits. JHEP **03**, 020 (2025). https://doi.org/10.1007/JHEP03(2025)020. arXiv:2412.01761
39. J.F. Gunion, H.E. Haber, G.L. Kane, S. Dawson, *The Higgs Hunter's Guide*, vol. 80 (2000)
40. Particle Data Group Collaboration, Review of particle physics (RPP). Phys. Rev. D **86**, 010001 (2012). https://doi.org/10.1103/PhysRevD.86.010001
41. J.A. Aguilar-Saavedra, Mixing with vector-like quarks: constraints and expectations. EPJ Web Conf. **60**, 16012 (2013). https://doi.org/10.1051/epjconf/20136016012. arXiv:1306.4432
42. V.D. Barger, M.S. Berger, R.J.N. Phillips, Quark singlets: implications and constraints. Phys. Rev. D **52**, 1663 (1995). https://doi.org/10.1103/PhysRevD.52.1663. arXiv:hep-ph/9503204
43. P.H. Frampton, P.Q. Hung, M. Sher, Quarks and leptons beyond the third generation. Phys. Rep. **330**, 263 (2000). https://doi.org/10.1016/S0370-1573(99)00095-2. arXiv:hep-ph/9903387
44. G. Barenboim, F.J. Botella, O. Vives, Constraining models with vector-like fermions from FCNC in K and B physics. Nucl. Phys. B **613**, 285 (2001). https://doi.org/10.1016/S0550-3213(01)00390-X. arXiv:hep-ph/0105306
45. J.A. Aguilar-Saavedra, Effects of mixing with quark singlets. Phys. Rev. D **67**, 035003 (2003). https://doi.org/10.1103/PhysRevD.69.099901. arXiv:hep-ph/0210112
46. S. Kanemura, M. Kikuchi, K. Yagyu, Fingerprinting the extended Higgs sector using one-loop corrected Higgs boson couplings and future precision measurements. Nucl. Phys. B **896**, 80 (2015). https://doi.org/10.1016/j.nuclphysb.2015.04.015. arXiv:1502.07716
47. L. Lavoura, J.P. Silva, The oblique corrections from vector-like singlet and doublet quarks. Phys. Rev. D **47**, 2046 (1993). https://doi.org/10.1103/PhysRevD.47.2046
48. C.-Y. Chen, S. Dawson, E. Furlan, Vectorlike fermions and Higgs effective field theory revisited. Phys. Rev. D **96**, 015006 (2017). https://doi.org/10.1103/PhysRevD.96.015006. arXiv:1703.06134
49. T. Hahn, Generating Feynman diagrams and amplitudes with FeynArts 3. Comput. Phys. Commun. **140**, 418 (2001). https://doi.org/10.1016/S0010-4655(01)00290-9. arXiv:hep-ph/0012260
50. J. Kublbeck, M. Bohm, A. Denner, Feyn arts: computer algebraic generation of Feynman graphs and amplitudes. Comput. Phys. Commun. **60**, 165 (1990). https://doi.org/10.1016/0010-4655(90)90001-H
51. T. Hahn, C. Schappacher, The Implementation of the minimal supersymmetric standard model in FeynArts and FormCalc. Comput. Phys. Commun. **143**, 54 (2002). https://doi.org/10.1016/S0010-4655(01)00436-2. arXiv:hep-ph/0105349
52. T. Hahn, M. Perez-Victoria, Automatized one loop calculations in four-dimensions and D-dimensions. Comput. Phys. Commun. **118**, 153 (1999). https://doi.org/10.1016/S0010-4655(98)00173-8. arXiv:hep-ph/9807565
53. S. Kanemura, T. Kubota, E. Takasugi, Lee–Quigg–Thacker bounds for Higgs boson masses in a two doublet model. Phys. Lett. B **313**, 155 (1993). https://doi.org/10.1016/0370-2693(93)91205-2. arXiv:hep-ph/9303263
54. A. Barroso, P.M. Ferreira, I.P. Ivanov, R. Santos, Metastability bounds on the two Higgs doublet model. JHEP **06**, 045 (2013). https://doi.org/10.1007/JHEP06(2013)045. arXiv:1303.5098
55. N.G. Deshpande, E. Ma, Pattern of symmetry breaking with two Higgs doublets. Phys. Rev. D **18**, 2574 (1978). https://doi.org/10.1103/PhysRevD.18.2574
56. W. Grimus, L. Lavoura, O.M. Ogreid, P. Osland, A precision constraint on multi-Higgs-doublet models. J. Phys. G **35**, 075001 (2008). https://doi.org/10.1088/0954-3899/35/7/075001. arXiv:0711.4022
57. M.J. Molewski, B.J.P. Jones, Scalable qubit representations of neutrino mixing matrices. Phys. Rev. D **105**, 056024 (2022). https://doi.org/10.1103/PhysRevD.105.056024. arXiv:2111.05401
58. D. Eriksson, J. Rathsman, O. Stal, 2HDMC: two-Higgs-doublet model calculator physics and manual. Comput. Phys. Commun. **181**, 189 (2010). https://doi.org/10.1016/j.cpc.2009.09.011. arXiv:0902.0851
59. P. Bechtle, D. Dercks, S. Heinemeyer, T. Klingl, T. Stefaniak, G. Weiglein et al., HiggsBounds-5: testing Higgs sectors in the LHC 13 TeV era. Eur. Phys. J. C **80**, 1211 (2020). https://doi.org/10.1140/epjc/s10052-020-08557-9. arXiv:2006.06007
60. P. Bechtle, S. Heinemeyer, T. Klingl, T. Stefaniak, G. Weiglein, J. Wittbrodt, HiggsSignals-2: probing new physics with precision Higgs measurements in the LHC 13 TeV era. Eur. Phys. J. C **81**, 145 (2021). https://doi.org/10.1140/epjc/s10052-021-08942-y. arXiv:2012.09197
61. H. Bahl, T. Biekötter, S. Heinemeyer, C. Li, S. Paasch, G. Weiglein et al., HiggsTools: BSM scalar phenomenology with new versions of HiggsBounds and HiggsSignals. Comput. Phys. Commun. **291**, 108803 (2023). https://doi.org/10.1016/j.cpc.2023.108803. arXiv:2210.09332
62. P. Bechtle, O. Brein, S. Heinemeyer, G. Weiglein, K.E. Williams, HiggsBounds: confronting arbitrary Higgs sectors with exclusion bounds from LEP and the Tevatron. Comput. Phys. Commun. **181**, 138 (2010). https://doi.org/10.1016/j.cpc.2009.09.003. arXiv:0811.4169
63. P. Bechtle, O. Brein, S. Heinemeyer, G. Weiglein, K.E. Williams, HiggsBounds 2.0.0: confronting neutral and charged Higgs sector predictions with exclusion bounds from LEP and the Teva-

tron. Comput. Phys. Commun. **182**, 2605 (2011). https://doi.org/10.1016/j.cpc.2011.07.015. arXiv:1102.1898
64. P. Bechtle, O. Brein, S. Heinemeyer, O. Stål, T. Stefaniak, G. Weiglein et al., HiggsBounds-4: improved tests of extended Higgs sectors against exclusion bounds from LEP, the Tevatron and the LHC. Eur. Phys. J. C **74**, 2693 (2014). https://doi.org/10.1140/epjc/s10052-013-2693-2. arXiv:1311.0055
65. P. Bechtle, S. Heinemeyer, O. Stal, T. Stefaniak, G. Weiglein, Applying exclusion likelihoods from LHC searches to extended Higgs sectors. Eur. Phys. J. C **75**, 421 (2015). https://doi.org/10.1140/epjc/s10052-015-3650-z. arXiv:1507.06706
66. ATLAS Collaboration, Exploration at the high-energy frontier: ATLAS Run 2 searches investigating the exotic jungle beyond the Standard Model. arXiv:2403.09292
67. CMS Collaboration Review of searches for vector-like quarks, vector-like leptons, and heavy neutral leptons in proton-proton collisions at $\sqrt{s} = 13$ TeV at the CMS experiment. arXiv:2405.17605
68. J. Alwall, R. Frederix, S. Frixione, V. Hirschi, F. Maltoni, O. Mattelaer et al., The automated computation of tree-level and next-to-leading order differential cross sections, and their matching to parton shower simulations. JHEP **07**, 079 (2014). https://doi.org/10.1007/JHEP07(2014)079. arXiv:1405.0301
69. T. Sjöstrand, S. Ask, J.R. Christiansen, R. Corke, N. Desai, P. Ilten et al., An introduction to PYTHIA 8.2. Comput. Phys. Commun. **191**, 159 (2015). https://doi.org/10.1016/j.cpc.2015.01.024. arXiv:1410.3012
70. DELPHES 3 Collaboration, DELPHES 3, a modular framework for fast simulation of a generic collider experiment. JHEP **02**, 057 (2014). https://doi.org/10.1007/JHEP02(2014)057. arXiv:1307.6346
71. M. Cacciari, G.P. Salam, G. Soyez, The anti-k_t jet clustering algorithm. JHEP **04**, 063 (2008). https://doi.org/10.1088/1126-6708/2008/04/063. arXiv:0802.1189
72. CMS Collaboration, Identification of b-Quark Jets with the CMS Experiment. JINST **8**, P04013 (2013). https://doi.org/10.1088/1748-0221/8/04/P04013. arXiv:1211.4462
73. NNPDF Collaboration, Parton distributions for the LHC Run II. JHEP **04**, 040 (2015). https://doi.org/10.1007/JHEP04(2015)040. arXiv:1410.8849
74. S. Hoeche, F. Krauss, N. Lavesson, L. Lonnblad, M. Mangano, A. Schalicke et al., Matching parton showers and matrix elements. In *HERA and the LHC: A Workshop on the Implications of HERA for LHC Physics: CERN - DESY Workshop 2004/2005 (Midterm Meeting, CERN, 11–13 October 2004; Final Meeting, DESY, 17-21 January 2005)*, pp. 288–289 (2005). https://doi.org/10.5170/CERN-2005-014.288. arXiv:hep-ph/0602031
75. M. Czakon, A. Mitov, Top++: a program for the calculation of the top-pair cross-section at hadron colliders. Comput. Phys. Commun. **185**, 2930 (2014). https://doi.org/10.1016/j.cpc.2014.06.021. arXiv:1112.5675
76. G. Bevilacqua, M. Czakon, C.G. Papadopoulos, R. Pittau, M. Worek, Assault on the NLO Wishlist: pp –> t anti-t b anti-b. JHEP **09**, 109 (2009). https://doi.org/10.1088/1126-6708/2009/09/109. arXiv:0907.4723
77. G. Bevilacqua, M. Lupattelli, D. Stremmer, M. Worek, Study of additional jet activity in top quark pair production and decay at the LHC. Phys. Rev. D **107**, 114027 (2023). https://doi.org/10.1103/PhysRevD.107.114027. arXiv:2212.04722
78. J.M. Campbell, R.K. Ellis, $t\bar{t}W^{+-}$ production and decay at NLO. JHEP **07**, 052 (2012). https://doi.org/10.1007/JHEP07(2012)052. arXiv:1204.5678
79. G. Bevilacqua, H.B. Hartanto, M. Kraus, J. Nasufi, M. Worek, NLO QCD corrections to full off-shell production of $t\bar{t}Z$ including leptonic decays. JHEP **08**, 060 (2022). https://doi.org/10.1007/JHEP08(2022)060. arXiv:2203.15688
80. D. Stremmer, M. Worek, Production and decay of the Higgs boson in association with top quarks. JHEP **02**, 196 (2022). https://doi.org/10.1007/JHEP02(2022)196. arXiv:2111.01427
81. G. Bevilacqua, M. Worek, Constraining BSM Physics at the LHC: four top final states with NLO accuracy in perturbative QCD. JHEP **07**, 111 (2012). https://doi.org/10.1007/JHEP07(2012)111. arXiv:1206.3064
82. Particle Data Group Collaboration, Review of particle physics. Phys. Rev. D **110**, 030001 (2024). https://doi.org/10.1103/PhysRevD.110.030001
83. G. Cowan, K. Cranmer, E. Gross, O. Vitells, Asymptotic formulae for likelihood-based tests of new physics. Eur. Phys. J. C **71**, 1554 (2011). https://doi.org/10.1140/epjc/s10052-011-1554-0. arXiv:1007.1727